JOURNAL OF GEOPHYSICAL RESEARCH, VOL. 112, D08303, doi:10.1029/2006JD007499, 2007

Polar mesospheric cloud mass and the ice budget: 3. Application of a coupled ice-chemistry-dynamics model and comparison with observations

David E. Siskind,[1] Mark Hervig,[2] Jörg Gumbel,[3] and Michael H. Stevens[1]

Received 11 May 2006; revised 27 November 2006; accepted 3 December 2006; published 20 April 2007.

[1] We have combined a two-dimensional chemical/dynamics model with a monodisperse parameterization of polar mesospheric clouds (PMCs) to study the interaction of PMCs with the climate of the summer mesopause region. First, we show that PMC absorption of terrestrial and solar IR radiation lead to atmospheric heating rates which can exceed 10 K/day. This heat is dissipated by increased upwelling above the cloud layer and by a 2–6 K temperature increase. We then calculate the global PMC ice mass and evaluate its sensitivity to IR heating, assumed particle size and level of solar activity. Inclusion of the temperature increase in the model can reduce the calculated ice mass by up to a factor of two. The calculated solar cycle range in the ice mass is also about a factor of two. The calculated latitude distribution and solar cycle range of PMC ice mass are in good agreement with recent analyses of PMC satellite data. Finally, we test the hypothesis that PMC formation leads to ozone changes by comparing our model with ozone data from the Halogen Occultation Experiment (HALOE). The data show a 20–30% ozone enhancement above PMCs. In the model, dehydration above the cloud layer leads to an ozone increase due to lowered HO_x. However, this competes with the temperature increase from IR absorption that can damp out this ozone increase. Surprisingly, for realistic estimates of the terrestrial IR flux, the model ozone response is reduced to well below that observed by HALOE.

Citation: Siskind, D. E., M. Hervig, J. Gumbel, and M. H. Stevens (2007), Polar mesospheric cloud mass and the ice budget: 3. Application of a coupled ice-chemistry-dynamics model and comparison with observations, *J. Geophys. Res.*, *112*, D08303, doi:10.1029/2006JD007499.

1. Introduction

[2] Since the late 19th century, polar mesospheric clouds (PMCs) have captured the interest of aeronomers for several reasons. First, they occur in one of the most extreme conditions of the Earth's atmosphere: the very cold summer mesopause [*Siskind et al.*, 2003]. Second, since there apparently is no mention of PMCs in the historical record before 1885 [*Thomas et al.*, 1989], there is speculation that their very existence is due to anthropogenic influences on middle atmospheric composition and climate.

[3] In order to address questions of PMC change over historical time scales, it is necessary to have an atmospheric model which couples the relative processes and accounts for possible interactions between PMCs and the environment in which they form. Recently there has been great interest in chemical effects from PMCs. For example, *von Zahn and Berger* [2003] suggested that the persistent dehydration associated with the deposition of water vapor to form PMCs could have a photochemical effect on radiatively active species such as ozone. *Murray and Plane* [2005] have also looked at the impact of PMC formation on trace chemical constituents. They used an imposed ice distribution and found that heterogeneous uptake of O on ice was slow and that the largest effects would be from the enhanced H_2O present at and below the cloud layer. Here we will show that observational effects can be present from both types of H_2O perturbations, the dehydration above the clouds and the enhancement below the clouds.

[4] One difficulty in achieving a coupled ice-chemistry-climate model lies in the complexity of performing detailed microphysical calculations in parallel with detailed chemistry and dynamics. We have recently discussed one approach to such a model [*Siskind and Stevens*, 2006] which offers considerable simplification of the detailed microphysics while retaining the essential radiative and photochemical feedbacks thought to occur from PMCs. In particular, we assumed that the particles were monodisperse, i.e., that all the ice particles were the same radius. This allowed us to evaluate the effect of the dehydration of H_2O leading to ozone increases as well as a small temperature rise. However, in that preliminary study, several questions were left

[1]Space Science Division, Naval Research Laboratory, Washington, D. C., USA.
[2]GATS, Inc., Driggs, Idaho, USA.
[3]Department of Meteorology, Stockholm University, Stockholm, Sweden.

0148-0227/07/2006JD007499$09.00

Report Documentation Page

Form Approved
OMB No. 0704-0188

1. REPORT DATE	2. REPORT TYPE	3. DATES COVERED
27 NOV 2006		**00-00-2006 to 00-00-2006**

4. TITLE AND SUBTITLE	5a. CONTRACT NUMBER
Polar mesospheric cloud mass and the ice budget: 3. Application of a coupled ice-chemistry-dynamics model and comparison with observations	5b. GRANT NUMBER
	5c. PROGRAM ELEMENT NUMBER
6. AUTHOR(S)	5d. PROJECT NUMBER
	5e. TASK NUMBER
	5f. WORK UNIT NUMBER
7. PERFORMING ORGANIZATION NAME(S) AND ADDRESS(ES) **Naval Research Laboratory,Space Science Division,4555 Overlook Avenue SW,Washington,DC,20375**	8. PERFORMING ORGANIZATION REPORT NUMBER
9. SPONSORING/MONITORING AGENCY NAME(S) AND ADDRESS(ES)	10. SPONSOR/MONITOR'S ACRONYM(S)
	11. SPONSOR/MONITOR'S REPORT NUMBER(S)

12. DISTRIBUTION/AVAILABILITY STATEMENT
Approved for public release; distribution unlimited

13. SUPPLEMENTARY NOTES

14. ABSTRACT

15. SUBJECT TERMS

16. SECURITY CLASSIFICATION OF:			17. LIMITATION OF ABSTRACT	18. NUMBER OF PAGES	19a. NAME OF RESPONSIBLE PERSON
a. REPORT	b. ABSTRACT	c. THIS PAGE			
unclassified	**unclassified**	**unclassified**	**Same as Report (SAR)**	**9**	

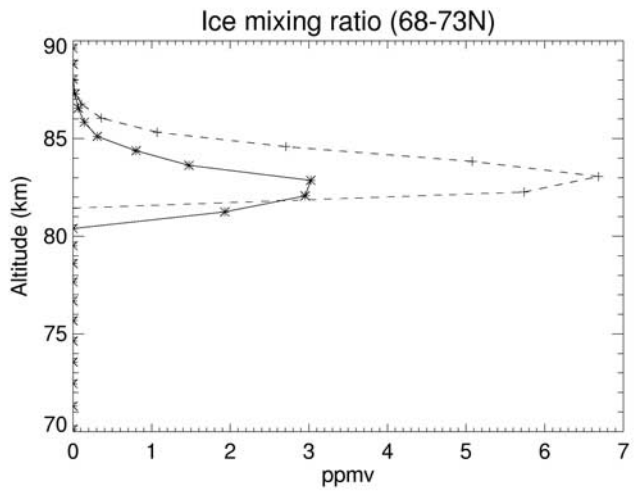

Figure 1. Calculated ice profiles for day 201 for 68–73°N. The solid line assumes a size of 70 nm, and the dashed line assumes 30 nm.

unanswered, namely possible direct heating by ice IR absorption effects and the uncertainty introduced by the selection of a single particle size. Furthermore, we did not consider how to test this model against observations.

[5] In this paper we develop the above ideas more fully. Our specific objectives are to first, consider the effect of ice particle heating on PMCs and the summer mesopause environment and, second, to better validate the predictions of this model by comparison with satellite data, both of PMCs and ozone. We will also evaluate the effects of particle size on the calculated ice distribution and consider solar cycle effects. This paper is one of a three part series of papers which address the PMC ice mass. The other two are *Englert et al.* [2007, hereinafter referred to as paper 1] and *Stevens et al.* [2007, hereinafter referred to as paper 2].

2. Modeling Approach

[6] As noted above, the *Siskind and Stevens* [2006] model assumes a single particle size. While this assumption precludes us from doing meaningful optical calculations as per *Siskind et al.* [2005], it does allow us to examine certain feedbacks of ice on the photochemistry and thermal balance that have heretofore remained unexplored. In our approach, water vapor is converted to ice when the saturation ratio, S, (= water vapor partial pressure over the saturation pressure for water over ice) exceeds 10. This is the deposition regime and the particle density can increase because of progressive deposition of water vapor. When $S < 1$, we are in the sublimation regime where ice converts back to water vapor. When S is between 1 and 10, neither particle growth or sublimation occurs and the ice particles are passively transported. The value of S is determined from the temperature and water vapor fields calculated by the NRL CHEM2D model [*Siskind et al.*, 2003, 2005]. The resulting ice is subject to diffusion and advection just as all the other model trace constituents. In addition, sedimentation is assumed to follow the formulae presented by *Reid* [1975] for spherical particles.

[7] For this work, we have made several changes to the *Siskind and Stevens* [2006] model. First, we now use the vapor pressure formulation of *Murphy and Koop* [2005], as recommended by *Rapp and Thomas* [2006] (their equation (4)). This leads to a reduction of about 30% in the total ice mass calculated by the model. Second, we have doubled the model's vertical resolution from 2 km to 1 km. Thus we now use a model which has 88 levels, spaced evenly in log-pressure coordinates, from the ground to about 115 km. The increased vertical resolution allows us now to examine more carefully the effects of our assumed particle size on PMC altitude. Figure 1 shows calculated ice profiles for day 201, for two assumed particle sizes, 30 nm and 70 nm, near 70°N latitude. The calculated ice abundance for the 30 nm case is larger, consistent with a slower fall speed into the warmer air. In terms of total ice content, the 30 nm profile here contains about 60% more ice than the 70 nm case, also consistent with the slower loss into warmer air. While both ice layers peak at about 82–83 km, the 70 nm layer extends lower in altitude by about 1 km, again consistent with more rapid sedimentation of the larger particles.

[8] The question of which particle size to use is controversial but inconsequential in our case. It is controversial because current estimates range from 20 to 120 nm (see papers 1 and 2) (and, as we do here, often assume spherical particles which *Eremenko et al.* [2005] show is probably not true). However, it is also inconsequential because the ultimate free parameter in the model is the gravity wave drag which controls the mesopause temperature. For example, in calculations we have done (not shown here) we find that an increase in the gravity wave forcing of 15–20%, which lowers our mesopause temperature by 2–3 K, is equivalent of changing the assumed particle size from 30 nm to 50 nm. We assume 30 nm as a baseline case (rather than the 70 nm used by *Siskind and Stevens* [2006]) since some of the more recent work [*von Savigny et al.*, 2005; *Rapp and Thomas*, 2006] suggest that is appropriate. Further our results apply to the ice as a whole, not merely those particles bright enough (and thus large enough) to be observed as clouds, so a bias to smaller sizes is probably appropriate. However we stress that the relative ozone changes we will report and the model variations with ice heating, latitude and solar activity are all relatively insensitive to the specific particle size we assume.

[9] Finally, and most importantly, we have tested a parameterization for the direct radiative heating due to ice particle absorption of terrestrial and solar IR. The motivation for this was the calculation of *Espy and Jutt* [2002] who showed significant heating of the ice particles over the ambient background air. However Espy and Jutt did not consider the possibility that the ice particles would heat the background air. Here we test this scenario in the limit that all absorbed radiation eventually serves as a heat source for the atmosphere, i.e., emission of thermal radiation from the particles and transfer into latent heat by sublimation are neglected. *Espy and Jutt* [2002, Figure 4] suggest that these are good assumptions for particles of order 50 nm radius and for temperatures below 160 K.

[10] Considering the thermal radiation available and the absorption features of ice, two spectral regions contribute mainly to this heating: terrestrial radiation in the wavelength range 10–14 microns and solar radiation around 3 microns.

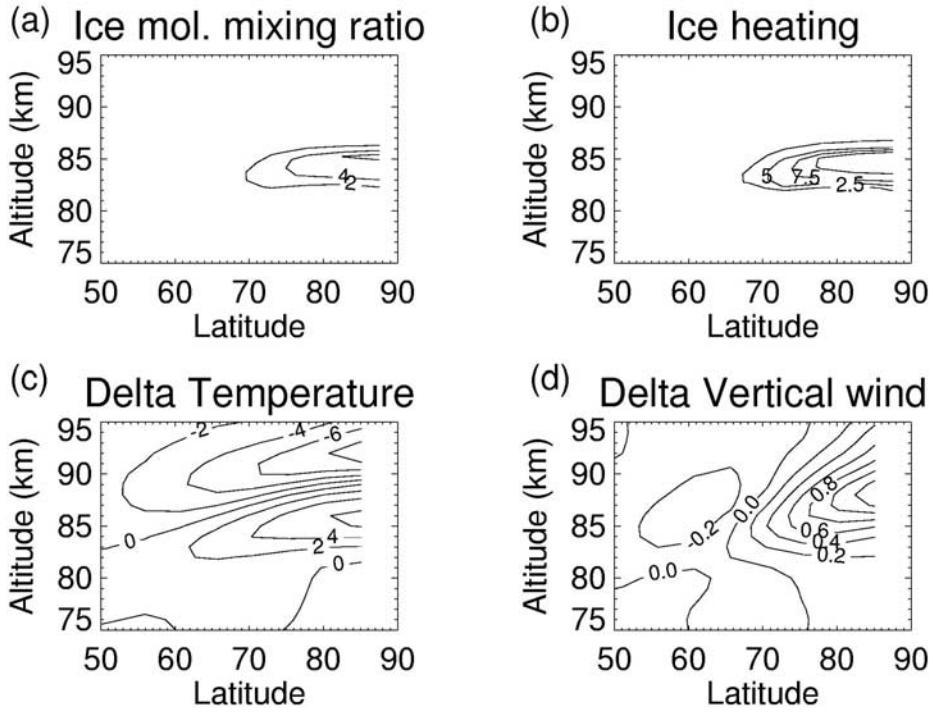

Figure 2. Effect of IR ice particle heating on the calculated temperature and vertical wind as a function of latitude (Northern Hemisphere) for day 201. Total ice heating ($P_{terr} + P_{sol}$) of 40 W cm^{-3} was assumed (see equations (1)–(3) and discussion therein). (a) Molecular ice mixing ratio (ppmv). Contours are every 2, with a peak just over 6 ppmv. (b) Resultant ice heating rate (K/day) according to equation (3). Contours are every 2.5 K/day, with a peak value around 11 K/day. (c) Temperature difference compared with a case of no ice heating. Contours are every 2 K. There is a localized peak of +6 K at 86 km and a decrease of −8 K at 92 km. (d) Difference in the vertical wind compared with a case of no ice heating. Contours are every 0.2 cm/s with a peak of 1.2 cm/s at 88 km.

This terrestrial radiation coincides with an atmospheric transmission window and, hence, the thermal flux is essentially determined by the emission temperature from either the surface or the top of the tropospheric cloud layer. The solar thermal flux is taken from *World Meteorological Organization* [1985]. To a good approximation, absorption of infrared radiation by PMC particles is governed by the Rayleigh regime and the absorption cross section scales with the particle volume [*van de Hulst*, 1981]. The absorbed infrared radiation in a PMC is therefore conveniently expressed per cloud ice volume. Applying the refractive indices from *Warren* [1984], we estimate the heating of the ice by solar near-infrared to be P_{sol} = 16 W cm^{-3} during the daytime (which is essentially 24 hours long for the upper mesosphere during the PMC season according to our calculations). For heating by terrestrial radiation, temperatures which range from 220 K (representative cloud top) to 263 K (surface ice and snow) up to 283 K (bare ground) yield P_{terr} values of 17, 41 and 56 W cm^{-3}, respectively. This illustrates the strong sensitivity of the total ice absorption to emission conditions in the lower atmosphere.

[11] If we ignore particle sublimation, the heating of the entire air parcel can be expressed as

$$dT/dt = (P_{terr} + P_{sol}) * V_{ice}/(c_p N_{air}) \quad (1)$$

where P_{terr} and P_{sol} are the numbers given above, c_p is the molecular heat capacity, V_{ice} is the fractional volume density and N_{air} is the number density of the air. For the purposes of inclusion in the 2-D model, it is desirable to reexpress (1) in terms of ice mixing ratio, μ_{ice}. Thus if we express V_{ice} as

$$V_{ice} = \frac{\mu_{ice} N_{air}}{(\rho_{ice}/M_{H_2O})} \quad (2)$$

substituting equation (2) into equation (1) eliminates N_{air} and after evaluating all the numerical constants (e.g., ρ_{ice} = 0.916 g cm^{-3}, and M_{H_20} = 2.98e-23 g) we obtain

$$dT/dt = 0.68 P_{tot} \mu_{ice} \quad (3)$$

where $P_{tot} = P_{terr} + P_{sol}$ and the numerical coefficient, 0.68 has units of cm^3/(J/K). With P_{tot} given in units of J s^{-1} cm^{-3} and μ_{ice} expressed in units of ppmv, equation (3) conveniently comes out in units of K s^{-1}. This heating is in addition to the photochemical heating from increased O_3 discussed by *Siskind and Stevens* [2006].

[12] Using this parameterization in CHEM2D we can evaluate the atmospheric response to this heat source. While the P_{terr} component of P_{tot} should properly be latitude-

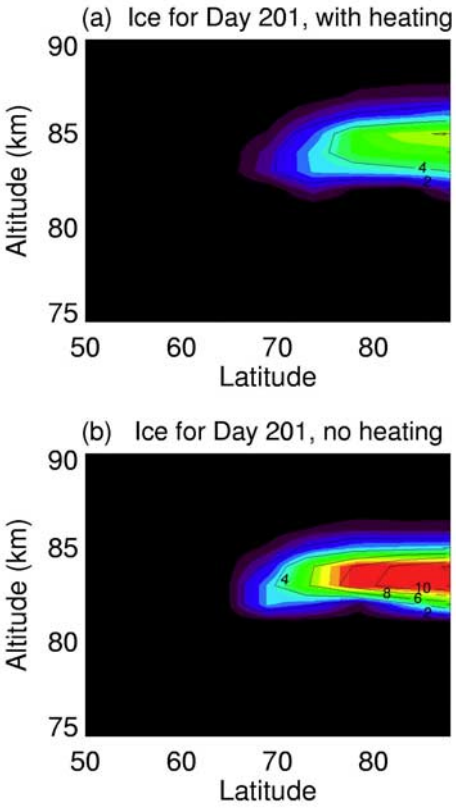

Figure 3. Calculated ice distributions (ppmv) and the effect of ice IR heating. (a) Accounts for ice particle heating as in Figure 2. (b) No feedback from ice particle heating.

dependent to account for surface albedo variations, in this work, which is only focused on establishing relative sensitivities, we do not account for this variation. Indeed, as we will show in subsequent figures, our model-data O_3 comparisons work best for values of P_{terr} which are quite low, probably too low, compared with our calculated range of 17–56 W cm^{-3}, discussed above. In anticipation of this result, the sensitivity studies use P_{terr} values which are on the low end of the calculated range. In all cases below, any calculation which includes ice particle heating always assumes P_{sol} = 16 W cm^{-3}.

[13] Figure 2 compares temperature and vertical wind differences from two simulations as a function of height and latitude, both assuming 30 nm particles, one with IR ice heating (P_{terr} = 24 W cm^{-3}) and one without. Also shown are the ice mixing ratio and the ice heating rate calculated using (3). At the altitude of the ice layer we see a general 2–6 K temperature increase. However, immediately above the ice layer there is a moderate increase in the vertical wind, up to 1.2 cm s^{-1}. This causes cooling above the mesopause, of up to 8 K. Thus the effects of the absorption of IR radiation by ice particles are seen to be partly thermal and partly dynamical. In terms of the effect on the calculated ice layer, the heating is most important and leads to significantly less ice. This is shown in Figures 3 and 4 which present different ways we have quantified the ice distribution.

[14] Figure 3 shows the calculated ice distribution, expressed as gas phase equivalent mixing ratio, for 20 July for the case with the same IR ice heating as in Figure 2a compared with a no-heating baseline (Figure 2b). The peak ice mixing ratio decreased from about 12 ppmv to 6 ppmv.

[15] Figure 4 shows the total vertically integrated ice mass as a function of latitude for the three model cases. We find this diagnostic [e.g., *Stevens et al.*, 2005; paper 2] to be particularly attractive for assessing the ice budget. It is convenient since it sidesteps the need to quantify occurrence frequency or optical properties such as albedo or backscatter ratio, none of which can be quantified by our parameterized approach. Figure 4 shows the calculated ice mass as a function of latitude for 3 model calculations with varying amounts of ice heating. All three cases assume a 30 nm ice particle radius and are for midseason conditions (typically mid-July for the model) and for solar conditions halfway between maximum and minimum. In general, for all model calculations, the ice mass increases sharply starting at 63°N (the model resolution is 4.8° of latitude), peaks between 73 and 78°N and falls off as one moves to the pole. This high-latitude falloff is simply from smaller global surface area near the pole; the actual ice mixing ratio peaks at the pole. The effect of even a modest amount of ice heating (up to P_{terr} = 24 W cm^{-3}, recall that we estimate it could peak at almost twice that if over bare ground) is to reduce the ice mass by a factor of two.

[16] For comparison, in Figure 4, we also show the ice mass estimated from observations by the Student Nitric Oxide Explorer (SNOE) satellite [*Bailey et al.*, 2005]. SNOE observed PMCs on the limb in both hemispheres between 1998 and 2003 up to 82° latitude. The derivation of the ice mass from the SNOE observations of PMC brightness and PMC frequency is given in papers 1 and 2. Consistent with those studies, we assumed a range of Gaussian ice particle size distributions with characteristic radii varying between 15 and 100 nm and widths from 10 to 20 nm. We assume the same particle size distribution constraints for the data collected at all latitudes shown. The shading in Figure 4 represents the area bounded by 95% of the

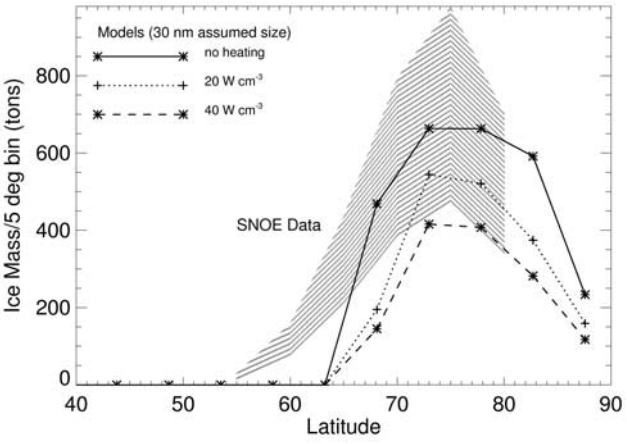

Figure 4. Ice mass (units are tons = 10^3 kg) versus latitude for three model ice heating rates ($P_{tot} = P_{sol} + P_{terr}$ = 0 (solid line with stars), 20 (dotted line with pluses) and 40 (dashed line with stars) W cm^{-3}) and SNOE data (grey scaling). As discussed in the text, P_{sol} is always fixed at 16 W cm^{-3}, and P_{terr} is the free parameter.

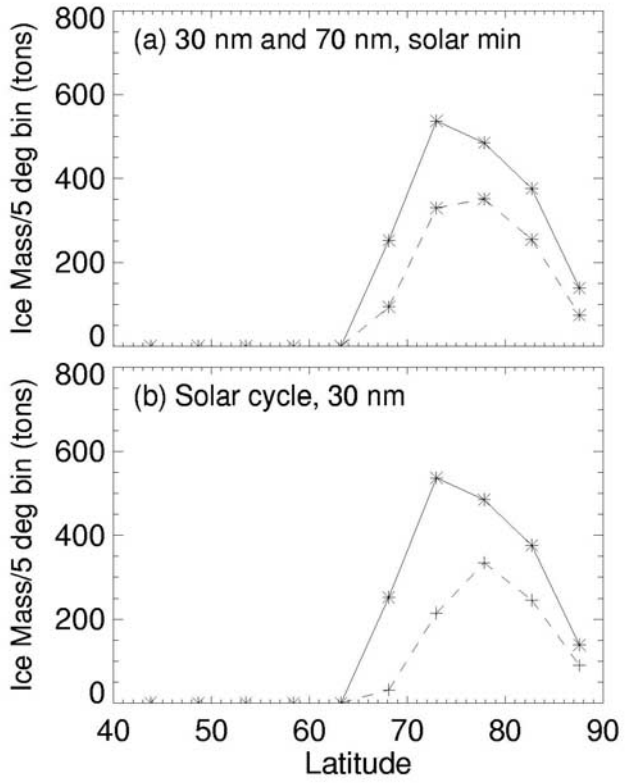

Figure 5. Similar to Figure 4 but for varying particle size and solar flux. All calculations assume 40 W cm^{-3} ice particle heating. (a) Effect of changes in assumed particle size (30 nm (solid) or 70 nm (dashed)) for a baseline solar minimum condition. (b) Effect of solar activity for a baseline particle size of 30 nm. The solid line is solar minimum, and the dashed is solar maximum.

solutions which result from our assumptions and is intended to reflect the uncertainties in the characteristics of the ice particle size distribution.

[17] In terms of the absolute value of the ice mass, one should exercise caution in interpreting the model data comparison. The model temperatures are driven by the gravity wave flux which is a free parameter; that is, the model can be made as cold as necessary. Plots such as Figure 4 (and Figure 5 to follow) are most useful for showing relative changes. Given that caveat, it is nonetheless interesting to see some of the model solutions (0 and 20 W cm^{-3} of heating) are in the range of the observations. Of course, with P_{sol} = 16 W cm^{-3}, the curve with P_{tot} = 20 W cm^{-3} implies a P_{terr} of only 4 W cm^{-3}, well below what we believe to be correct. This result might be robust since as we will see below, our O_3 comparisons suggest something similar. Another result that is likely to be robust is that at latitudes below 70°N, all the models fall below the observations. This is because, while our model temperature minimum at 70°N is 130 K, (in good agreement with the *Lübken* [1999] climatology), our model temperature minimum at 60°N is 149 K. While this is in good agreement with the 3-D model results of *Berger and von Zahn* [1999], it is too warm to form ice clouds. Given the sporadic nature of PMCs at latitudes equatorward of 65–70°N, it is likely that their occurrence reflects meteorological variability and associated sporadic cooling or transport events which are not in our highly truncated 2-D model. *Berger and Lübken* [2006] have recently presented the same argument using a three-dimensional model. Given the even simpler meteorology in the 2-D model, it is no surprise that our model does not have clouds in this region either.

[18] It is useful to compare the ice mass variations shown in Figure 4 with those from other free parameters in our model, namely the assumed particle size and the level of solar activity (see *Siskind et al.* [2005] for a discussion of how the solar cycle is handled in the model). These are shown in Figure 5 and also summarized, in a globally integrated sense, in Table 1. Table 1 shows that the calculated ice is largest for the case with 30 nm particles at solar minimum without any feedback from ice particle heating. The effect of going from an assumed size of 70 to 30 nm is to increase the calculated ice by about 35–40%. The effect of solar activity integrated over the entire NH is about a factor of two in total ice mass, roughly equivalent to the other variables tested.

[19] The general agreement between model and data in the solar cycle variation [e.g., paper 2, Figure 7] is satisfying, but perhaps not surprising given the general agreement between the model and HALOE in the solar cycle temperature change [*Hervig and Siskind*, 2006], which is the primary driver of PMC variability in the model. In summary, this section shows that for reasonable values of mesospheric temperature and water [*Siskind et al.*, 2005], and with reasonable assumptions as to mean particle diameter and ice heating, that our approach gives a good representation of the observations. The effect of IR ice heating is introduced as an important new variable that is as significant as the assumed particle size or level of solar activity.

3. Comparison With HALOE Ozone Observations

[20] A key prediction of the interactive PMC model as first described by *Siskind and Stevens* [2006] is that the ozone should increase in the dehydrated region above the clouds. This is a consequence of the anticorrelation between ozone and odd hydrogen [*Marsh et al.*, 2003]. Here we test that prediction with HALOE data and also look at the complications introduced by considering ice IR absorption.

[21] HALOE ozone is an attractive observational diagnostic for this purpose because good retrievals are available up to 90 km, well above the PMC region. *McHugh et al.* [2003] described a version of the HALOE data (Vpmc) which included corrections for PMC contamination. These corrections are based on an extrapolation of the measured

Table 1. Summary of Calculated Ice Mass

Number	Assumed Particle Radius, nm	Solar Flux	IR Heating, W cm^{-3}	Calculated Ice Mass, metric tons
1	70	minimum	0	1680
2	30	minimum	0	3440
3	70	maximum	0	910
4	30	maximum	0	1820
5	30	minimum	40	1800
6	30	maximum	40	950

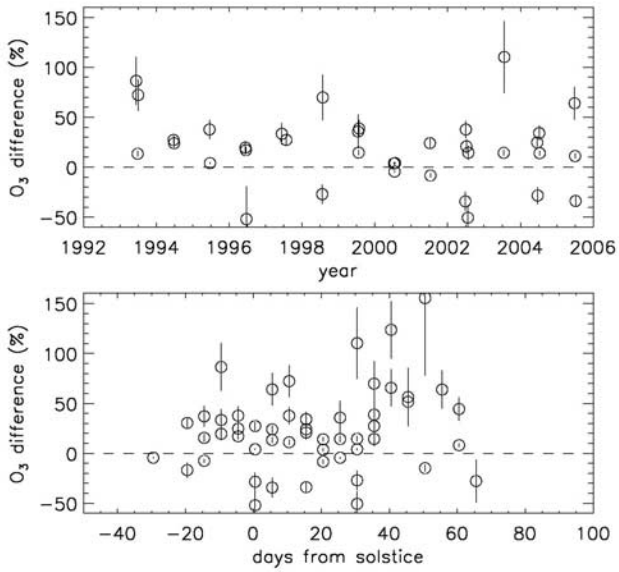

Figure 6. HALOE ozone differences in percent between air with a PMC and clear air, referenced to the clear air values, at a single altitude (85.2 km, about 0.0035 hPa). Each circle represents an average difference for a 5 day bin. (top) All the bins, sorted according to year. (bottom) All bins sorted by days from solstice, regardless of the year.

PMC extinction at 3.40 microns wavelength to the ozone channel wavelength at 9.87 microns. The extrapolations are based on modeled extinction ratios considering the temperature dependence of the ice refractive index from 130 to 210 K as described by *Clapp et al.* [1995]. In all cases, the extinction ratios are insensitive to particle size for the HALOE wavelengths and typical PMC radii. In the case of O_3, the extinction ratios are relatively insensitive to temperature, varying by less than 15% for temperatures less than 165 K.

[22] Figure 6 shows the effect of PMCs on O_3 using HALOE observations to compare clear-sky events with profiles containing PMCs. PMCs were identified using the threshold approach described by *Hervig et al.* [2003]. Measurements during 1991–2005 within the core summer season (−10 to 40 days from solstice) at latitudes from 60 to 70°N were examined. This period was divided up into bins of 5 days and 10° in latitude. There are thus up to 20 such bins per year. With consideration of duty cycle reductions, we have a total of 160 bins over the 14 year period. Of these, 23% have both PMC and clear air scans and this subset (37 total) is used to isolate the effect of ozone changes due to PMCs. The data in Figure 6 are ozone differences for latitude-time bins with both PMC and clear air measurements, referenced to the clear air value, from the 60–70°N latitude range, for pressures near .0035 hPa (corresponding to about 85 km). Figure 6 (top) is for the core part of the PMC season (−10 to +40 days from solstice) as a function of year; Figure 6 (bottom) includes the extra data from outside this core part of the season. Our idea of a core season is from the data of *Hervig et al.* [2003] which suggest relatively constant H_2O and ice from mid-June until 1 August. The error bars on each data point represent the error of the mean value of the fractional difference in each bin. The ozone standard deviation within each bin is about 65%. This variance contains both geophysical and instrumental components, thus the measurement uncertainty for individual ozone profiles is less than 65%. Taken together, both panels in Figure 6 show considerable scatter without any clear solar cycle or long-term trend. It is nonetheless clear, however, that most of the points show more ozone in the presence of PMCs than in clear air (i.e., the fractional differences are mostly positive).

[23] Figure 7 shows the HALOE results, averaged over 14 years, as a function of altitude. The red shading represents the error of the mean fractional ozone difference taken from averaging the data represented by that shown in Figure 6, at all altitudes. The data show a clear region where the ozone is enhanced above the cloud layer (PMCs typically exist between .003 and .006 hPa) and also a suggestion of a region below the cloud layer where ozone is reduced. The enhancement corresponds to the dehydrated region, the decrease corresponds to the region where H_2O is released upon sublimation. In addition, three profiles from the model are also shown. The latitude bands are 63–73°N for the model. The models were all run for a solar activity level which was an average between maximum and minimum conditions. Each of the three calculations assumed a different IR ice power density, either 0, 20 or 40 W cm^{-3}. Qualitatively the model curves show similar features as the data, but with some important quantitative differences. The largest ozone response is for the case with no IR absorption at all, the weakest is for the 40 W cm^{-3} case.

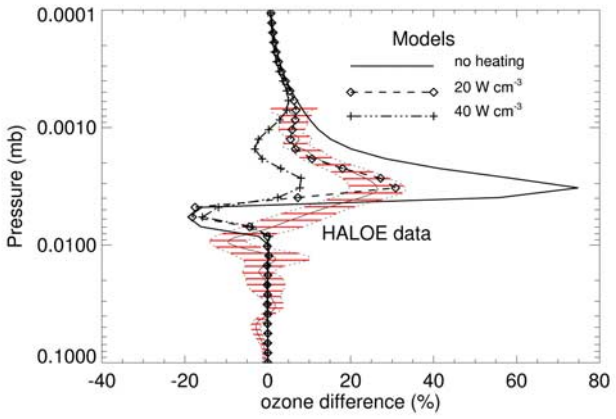

Figure 7. Comparison of HALOE and model ozone differences (PMC-clear air)/(clear air) as a function of pressure for mid-July. The data are for 60–70°N, and the models are for 63–73°N. The horizontal bars represent the 1-sigma range of the data. The solid line is for the model with no assumed ice particle heating. The dashed line with diamonds, which overlaps closest with the data, is a model with $P_{tot} = P_{sol} + P_{terr} = 20$ cm^{-3}; the dashed curve with pluses is a model with $P_{tot} = 40$ cm^{-3} (P_{sol} is always fixed at 16 cm^{-3}, see Figures 2 and 4 and text). The peak HALOE difference of 27 ± 7% corresponds to the average of the data shown in Figure 6. Clouds occur in the pressure region between 0.003 and 0.006 hPa; these pressures correspond roughly to altitudes between 82 and 85 km.

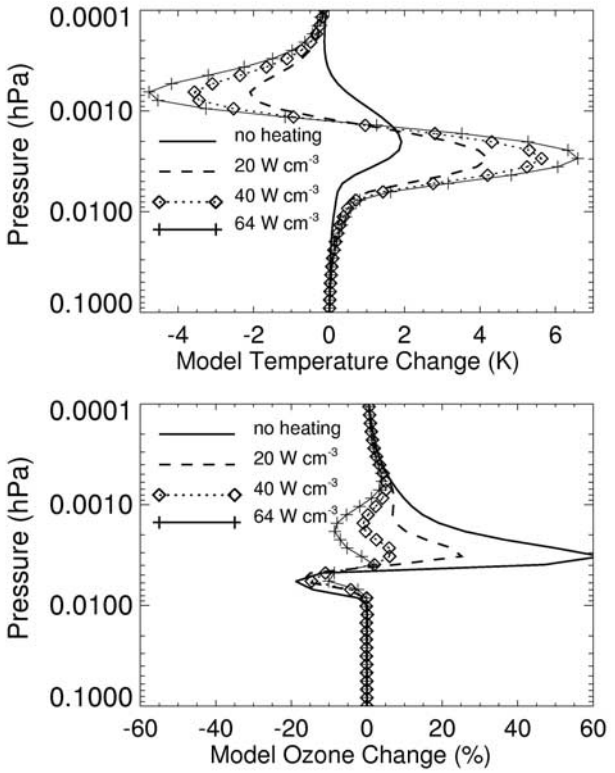

Figure 8. Sensitivity of model (top) temperature and (bottom) ozone to variations in assumed IR absorption by ice. The solid line is for no heating and produces the smallest temperature response and the largest ozone response. The long dashes are for $P_{tot} = P_{sol} + P_{terr} = 20$ W cm^{-3}, the short dashes with diamonds are for 40 W cm^{-3} and the solid line with pluses is for 64 W cm^{-3}. As with Figure 7, clouds occur in the pressure region between 0.003 and 0.006 hPa; these pressures correspond roughly to altitudes between 82 and 85 km.

[24] Figure 8 shows that the reason increased IR heating suppresses the ozone response is due to the temperature response. Both the model temperature and ozone respond to varying amounts of IR absorption. For the case with zero IR absorption, the temperature increase is relatively modest and solely due to increased ozone absorption [*Siskind and Stevens*, 2006]. For this case, the ozone increase is largest. As increasing amounts of IR absorption are assumed in the model, the temperature perturbation goes up and the ozone increase eventually disappears. This is a reflection of the well known anticorrelation between ozone and temperature [*Jucks and Salawitch*, 2000]. We thus have two competing processes, the Ox-HOx anticorrelation and the ozone-temperature anticorrelation. When the temperature increase is large enough, it cancels out the HOx decrease due to dehydration.

[25] What is unexpected about Figure 7 is that the model most consistent with the HALOE ozone assumes a very low, possibly unrealistically low IR flux. Recall that the solar NIR component alone provides 16 W cm^{-3} to the ice. The terrestrial component, even for a very cold emission temperature of 220 K, provides an additional 17 W cm^{-3}. For higher emission temperatures, the terrestrial component can be as high as 46 W cm^{-3}. The 20 W cm^{-3} total absorption which is the best model solution would therefore appear to be outside the range of acceptable terrestrial IR fluxes. Note that we have performed sensitivity studies using various ice refractive indices [e.g., *Warren*, 1984; *Toon et al.*, 1994; *Bertie et al.*, 1969; *Clapp et al.*, 1995] and the resulting heating changed by no more than 15%. We have also examined the ozone response to changing solar conditions and assumed particle size and found much smaller impact than the ice heating effects shown here.

[26] Thus while we feel that the ozone perturbations shown in Figures 6 and 7 represent the first unambiguous detection of the large-scale effects of dehydration and ice cloud sublimation on the chemistry of the mesopause region, the fact that the model which agrees best with the data assumes an unacceptably low IR absorption is a puzzle to be addressed. One possibility is that the CHEM2D model, as a diurnally averaged model, is not adequately capturing ozone responses to HOx and temperature which may depend upon the time of day.

[27] To test the uncertainties in this aspect of the comparison, we took two H_2O profiles from CHEM2D, one from the no-ice solar minimum case and the other from the 30 nm solar minimum case (similar to the H_2O shown by *Siskind and Stevens* [2006]) and used these profiles as input to a diurnal photochemical model [*Summers et al.*, 2001]. Figure 9 shows the ozone difference between these two calculations as a function of local time. Of specific interest is that the relative strength of the ozone enhancement and depletions vary by large amounts during the course of the day. This cannot be captured by the diurnally averaged CHEM2D model. The HALOE data were all taken either after 2000 hours or before 0400 hours. From Figure 9, it appears that the response of O_3 to an H_2O change is largest at these times. Thus it may not be surprising that the HALOE O_3 response exceeds the model for higher and

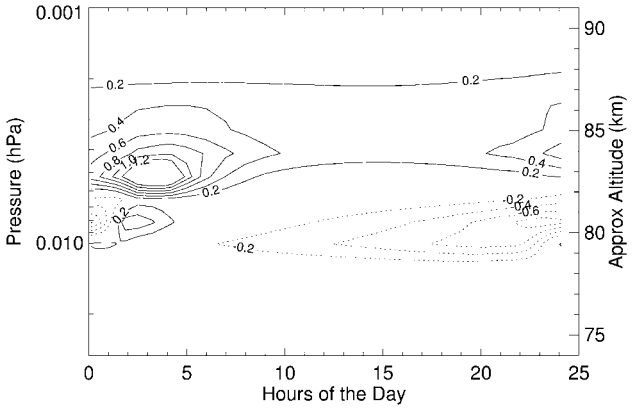

Figure 9. Sensitivity of ozone to dehydration as a function of local time for 68°N in July. The solid contours show regions of fractional ozone increases (referenced to the no-PMC case) greater than 0.2. The dotted contours show regions of fractional ozone decreases greater than 0.2. The region of increase is associated with dehydration at and above the cloud layer. The region of decrease is associated with enhanced H_2O from PMC sublimation.

more realistic IR fluxes. Of course, the heating and temperature likely change throughout the day and this is not captured in the 1-D model. An exact calculation should couple the radiative, chemical and dynamical processes in a full diurnal manner.

4. Conclusions

[28] We have applied an interactive PMC model to study several problems relating to the distribution of PMCs, their variability and their feedback on their background environment. Despite the simplicity of the parameterized microphysics we were able to highlight some new phenomena and obtain realistic PMC variations. This model accounts for two radiative feedbacks by PMCs on their background environment. The first feedback mechanism, from ozone heating resulting from dehydration was presented by *Siskind and Stevens* [2006]. The second, direct heating by ice absorption of IR radiation was presented for here for the first time. Heating by the ice particles can raise the model temperature by 2–6 K in the vicinity of the ice layer and lower the calculated ice mass by over 30–50%. For reasonable values of model temperature and water vapor, we get ice mass values which are in reasonable agreement with the analysis of PMC observations from the SNOE satellite [papers 1 and 2]. We get variations with solar activity that are also in general agreement with SNOE. This is consistent with previously published results [*Hervig and Siskind*, 2006] suggesting that the model temperature variation from solar minimum to maximum is at least approximately correct.

[29] We have also validated our model predictions with comparison with HALOE observations of ozone in the presence and absence of clouds. This has provided the first quantitative demonstration from satellite data of the effect of PMCs on a radiatively and photochemically active constituent. Both model and data show a clear ozone increase above the cloud layer. This is due to the anticorrelation of Ox and HOx. However, the ozone response is also seen to vary inversely with the assumed IR heating of the ice. One puzzle is that values of IR heating which seem most reasonable, based upon tropospheric emission temperatures, lead to too little ozone change. However, the uncertainties inherent in our highly parameterized approach to PMC modeling, as well as the limitations of comparing a diurnally averaged model with occultation data suggest that one should not expect an exact comparison.

[30] The sensitivity of PMCs, ozone and temperature to the IR flux from the lower atmosphere should open up several new areas of inquiry. First, a better validation of our results, specifically with higher-quality temperature data, should come from the SOFIE instrument on NASA's upcoming Aeronomy of Ice in the Mesosphere (AIM) mission. Second, *Espy and Jutt* [2002] have already pointed out the possibility of geographic variations in PMC formation due to varying lower atmospheric IR albedo. Our results support their idea and further suggest that analogous variations in ozone and temperature may also occur. A three-dimensional model would be most appropriate to explore this.

[31] **Acknowledgments.** We thank Chris Englert for helpful discussions and the HALOE science team for their effort in producing a fine data product. Funding was provided by NRL internal funding (from the Office of Naval Research) and the NASA Living with a Star program.

References

Bailey, S. M., A. W. Merkel, G. E. Thomas, and J. N. Carstens (2005), Observations of polar mesospheric clouds by the Student Nitric Oxide Explorer, *J. Geophys. Res.*, *110*, D13203, doi:10.1029/2004JD005422.

Berger, U., and F.-J. Lübken (2006), Weather in mesospheric ice layers, *Geophys. Res. Lett.*, *33*, L04806, doi:10.1029/2005GL024841.

Berger, U., and U. von Zahn (1999), The two-level structure of the mesopause: A model study, *J. Geophys. Res.*, *104*, 22,083–22,093.

Bertie, J. E., H. J. Labbe, and E. Whalley (1969), Absorptivity of ice in the range 4000–30 cm^{-1}, *J. Chem. Phys.*, *50*, 4501–4520.

Clapp, M. L., R. E. Miller, and D. R. Worsnop (1995), Frequency-dependent optical constants of water ice obtained directly from aerosol extinction spectra, *J. Phys. Chem.*, *99*, 6317–6326.

Englert, C. R., M. H. Stevens, and M. T. DeLand (2007), Polar mesospheric cloud mass and the ice budget: 1. Quantitative interpretation of mid-UV cloud brightness observations, *J. Geophys. Res.*, *112*, D08204, doi:10.1029/2006JD007533.

Eremenko, M. N., S. V. Petelina, A. Y. Zasetsky, B. Karlsson, C. P. Rinsland, E. J. Llewellyn, and J. J. Sloan (2005), Shape and composition of PMC particles derived from satellite remote sensing measurements, *Geophys. Res. Lett.*, *32*, L16S06, doi:10.1029/2005GL023013.

Espy, P. J., and H. Jutt (2002), Equilibrium temperature of water-ice aerosols in the high latitude summer mesosphere, *J. Atmos. Sol. Terr. Phys.*, *64*, 1823–1832.

Hervig, M., and D. Siskind (2006), Decadal and inter-hemispheric variability in polar mesospheric clouds, water vapor, and temperature, *J. Atmos. Sol. Terr. Phys.*, *68*, 30–41.

Hervig, M., M. McHugh, and M. Summers (2003), Water vapor enhancement in the polar summer mesosphere and its relationship to polar mesospheric clouds, *Geophys. Res. Lett.*, *30*(20), 2041, doi:10.1029/2003GL018089.

Jucks, K., and R. J. Salawitch (2000), Future changes in upper stratospheric ozone, in *Atmospheric Science Across the Stratopause*, *Geophys. Monogr. Ser.*, vol. 123, edited by D. E. Siskind et al., pp. 241–255, AGU, Washington, D. C.

Lübken, F.-J. (1999), Thermal structure of the Arctic summer mesopause, *J. Geophys. Res.*, *104*, 9135–9149.

Marsh, D., A. Smith, and E. Noble (2003), Mesospheric O_3 response to changes in water vapor, *J. Geophys. Res.*, *108*(D3), 4109, doi:10.1029/2002JD002705.

McHugh, M., M. Hervig, B. Magill, R. E. Thompson, E. Remsberg, J. Wrotny, and J. Russel III (2003), Improved mesospheric temperature, water vapor and polar mesospheric cloud extinctions from HALOE, *Geophys. Res. Lett.*, *30*(8), 1440, doi:10.1029/2002GL016859.

Murphy, D. M., and T. Koop (2005), Review of the vaopur pressure of ice and supercooled water for atmospheric applications, *Q. J. R. Meteorol. Soc.*, *131*, 1539–1565.

Murray, B. J., and J. M. C. Plane (2005), Modelling the impact of noctilucent cloud formation on atomic oxygen and other minor constituents of the summer mesosphere, *Atmos. Chem. Phys.*, *5*, 1027–1038.

Rapp, M., and G. E. Thomas (2006), Modeling the microphysics of mesospheric ice particles: Assessment of current capabilities and basic sensitivities, *J. Atmos. Sol. Terr. Phys.*, *68*, 715–744.

Reid, G. C. (1975), Ice clouds at the summer polar mesopause, *J. Atmos. Sci.*, *12*, 523–535.

Siskind, D. E., and M. H. Stevens (2006), A radiative feedback from an interactive polar mesospheric cloud parameterization in a two dimensional model, *Adv. Space Res.*, *38*(11), 2383–2387, doi:10.1016/j.asr.2005.03.094.

Siskind, D. E., S. D. Eckermann, J. P. McCormack, M. J. Alexander, and J. T. Bacmeister (2003), Hemispheric differences in the temperature of the summertime stratosphere and mesosphere, *J. Geophys. Res.*, *108*(D2), 4051, doi:10.1029/2002JD002095.

Siskind, D. E., M. H. Stevens, and C. R. Englert (2005), A model study of global variability in mesospheric cloudiness, *J. Atmos. Sol. Terr. Phys.*, *67*, 501–513.

Stevens, M. H., C. R. Englert, M. T. DeLand, and M. Hervig (2005), The polar mesospheric cloud mass in the Arctic summer, *J. Geophys. Res.*, *110*, A02306, doi:10.1029/2004JA010566.

Stevens, M. H., C. R. Englert, M. T. DeLand, and S. M. Bailey (2007), Polar mesospheric cloud mass and the ice budget: 2. Application to satellite data sets, *J. Geophys. Res.*, *112*, D08205, doi:10.1029/2006JD007532.

Summers, M. E., R. R. Conway, C. R. Englert, D. E. Siskind, M. H. Stevens, J. M. Russell III, L. L. Gordley, and M. J. McHugh (2001), Discovery of a water vapor layer in the Arctic summer mesosphere: Implications for polar mesospheric clouds, *Geophys. Res. Lett.*, *28*, 3601–3604.

Thomas, G. E., J. J. Olivero, E. J. Jensen, W. Schröder, and O. B. Toon (1989), Relation between increasing methane and the presence of ice clouds at the mesopause, *Nature*, *338*, 490–492.

Toon, O. B., M. A. Tolbert, B. G. Koehler, A. M. Middlebrook, and J. Jordan (1994), Infared optical constants of H_2O ice amorphous nitric acid solutions, and nitric acid hydrates, *J. Geophys. Res.*, *99*, 25,631–25,634.

van de Hulst, H. C. (1981), *Light Scattering by Small Particles*, Dover, Mineola, N. Y.

von Savigny, C., S. V. Petelina, B. Karlsson, E. J. Llewellyn, D. A. Degenstein, N. D. Lloyd, and J. P. Burrows (2005), Vertical variation of NLC particle sizes retrieved from Odin/OSIRIS limb scattering observations, *Geophys. Res. Lett.*, *32*, L07806, doi:10.1029/2004GL021982.

von Zahn, U., and U. Berger (2003), Persistent ice cloud in the midsummer upper mesosphere at high latitudes: Three-dimensional modeling and cloud interaction with ambient water vapor, *J. Geophys. Res.*, *108*(D8), 8451, doi:10.1029/2002JD002409.

Warren, S. G. (1984), Optical constants of ice from the ultraviolet to the microwave, *Appl. Opt.*, *23*, 1206–1225.

World Meteorological Organization (1985), Atmospheric ozone 1985: World Meteorological Organization Global Ozone Research and Monitoring Project, *Rep. 16*, Geneva, Switzerland.

J. Gumbel, Department of Meteorology, Stockholm University, SE-10691 Stockholm, Sweden.

M. Hervig, GATS, Inc., Driggs, ID 83422, USA.

D. E. Siskind and M. H. Stevens, Space Science Division, Naval Research Laboratory, Washington, DC 20375-5320, USA.